JCTC Journal of Chemical Theory and Computation

Magnetostructural Dynamics from Hubbard-*U* Corrected Spin-Projection: [2Fe−2S] Complex in Ferredoxin

Nisanth N. Nair,*,† Jordi Ribas-Arino, Volker Staemmler, and Dominik Marx

Lehrstuhl für Theoretische Chemie, Ruhr-Universität Bochum, 44780 Bochum, Germany

Received October 16, 2009

Abstract: A Hubbard-corrected spin-projected two-determinant approach, EBS+U_{scf}, is introduced to treat low-spin ground states of antiferromagnetically coupled transition metal complexes. In addition to providing access to total energies, forces, and ab initio simulations, it allows one to readily compute Heisenberg's exchange coupling $J(t)$ on the fly. By studying the binuclear [2Fe−2S] cofactor in a metalloprotein, *Anabaena* Fd, within this consistent nonempirical procedure in combination with a QM/MM framework, it is illustrated that spin-projection, self-interaction corrections, thermal fluctuations, and protein matrix shifts are crucial in obtaining $\langle J \rangle$ close to the experiment.

1. Introduction

The interplay of magnetic interactions and geometric structure[1] is at the heart of many important phenomena ranging from strongly correlated materials,[2] via transition metal coordination chemistry[3] to the redox biophysics of iron−sulfur proteins.[4] However, the computation of the magnetic exchange coupling constant J for even rather small transition metal complexes, which is crucial for describing magnetic clusters,[5–7] molecular magnets,[8] and metalloproteins,[9–11] to name but a few, is still a challenge to electronic structure calculations.[12] This applies to wave function-based methods because the computational complexity rapidly explodes beyond feasibility, although it is well-known what should be done in the systematic world of configuration interaction (CI) calculations. For instance, even the computation of J for the small antiferromagnetic $[Fe_2S_2(SH)_4]^{2-}$ complex in vacuo, being the most stripped-down model for the [2Fe−2S] cofactor in Ferredoxins (Fd) as a major class of mobile electron carrier in contemporary biology, is beyond current capabilities when it comes to convergence of multireference character, electron correlation, and basis set in concert.

The roots of the problem are quite different in the realm of density-based methods where conceptual difficulties dominate. It is well-known that LDA or GGA functionals suffer severely from spurious self-interactions,[13] producing artificially delocalized spin densities. This, in turn, induces stronger bonding, contraction of structures, and a dramatic overestimation of $|J|$.[14] This problem can be tackled in various ways such as using approximate self-interaction corrections[15–17] or hybrid functionals[14,18,19] including the idea to tune the admixture of Fock exchange appropriately.[20] In addition, constrained density functional theory[21] has been transferred successfully from solids to molecular systems[22–26] by controlling spin-density in real space.

A distinctly different route is to invoke a Hubbard-U correction.[27,28] In practice, this can be carried out by adjusting U (semi)empirically or by determining it self-consistently,[29] U_{scf}, using linear-response theory.[30] The GGA+U_{scf} method yields favorable results without any fit to experimental data at computational costs that are basically the same as those of the underlying GGA calculation in addition to allowing readily for ab initio molecular dynamics.[29,31–33]

All aforementioned density-based approaches draw on the idea to improve a single-determinantal representation of the antiferromagnetic ground state of such spin-coupled systems. A conceptually different approach to compute J is based on spin-projection schemes and relies on evaluating more than one total energy[34–36] and thus using more than one Kohn−Sham (KS) determinant. Along such lines, the "extended broken symmetry" (EBS) approach has been introduced,[37,38] which provides a general and efficient two-determinantal formulation of the antiferromagnetic low-spin

* Corresponding author e-mail: nnair@iitk.ac.in.

† Present address: Department of Chemistry, Indian Institute of Technology Kanpur, Kanpur 208016, India.

10.1021/ct900547w
Published on Web 01/15/2010

state of transition metal dimers. The EBS approach allows one to compute both geometrical structures and J values consistently by using identical spin-projection techniques. In addition, it can be easily used in ab initio molecular dynamics, thus opening the doorway to compute spectral densities $J(\omega)$ from the time evolution of the exchange coupling constant, $J(t)$, and thus to "magnetostructural dynamics".[37,38]

Here, we propose a technique, EBS+U_{scf}, that builds on the strengths of a systematic spin-projection scheme, EBS, combined with a linear-response GGA+U_{scf} treatment of the underlying open-shell KS determinants. Most importantly, this method is very practical and has the accuracy of state-of-the-art multireference CI calculations. In addition, being readily amenable to ab initio molecular dynamics,[39] EBS+U_{scf} provides access to the dynamics of magnetic properties. Here, this will be demonstrated by investigating the [2Fe−2S] cofactor in *Anabaena* Ferredoxin (Fd) within a QM/MM framework.[39]

2. Methods

2.1. Evaluation of Magnetic Exchange Coupling Constants. The magnetic properties of transition metal dimers may be represented by a Heisenberg Hamiltonian:

$$\hat{H} = -2J\hat{S}_A\hat{S}_B \tag{1}$$

where $\hat{S}_A$ and $\hat{S}_B$ are effective local spin angular momentum operators at the two sites A and B, respectively; $J < 0$ ($J > 0$) implies antiferromagnetic (ferromagnetic) coupling. J can be expressed[37] as

$$J = \frac{E^{BS} - E^{HS}}{S^2_{max} - S^2_{min} - \Theta^{BS} + \Theta^{HS}} \tag{2}$$

upon invoking generalized spin-projection ideas in conjunction with Löwdin's exact formulation of the expectation value of the total spin operator $\hat{S} = \hat{S}_A + \hat{S}_B$. Here, $S_{min} = |S_A - S_B|$ and $S_{max} = S_A + S_B$ are the minimum and maximum total spin quantum number corresponding to the exact high-spin (HS) and low-spin (LS) eigenstates of eq 1, respectively. E^{HS} and E^{BS} are the total energies of the HS and broken symmetry (BS) states obtained using spin-polarized KS determinants with appropriate integer occupation numbers. Because these determinants are not spin eigenfunctions, they contain spin contaminations that are generally different for the different spin states. However, the expression for J in eq 2 contains systematic corrections for these spin contaminations via

$$\Theta^X = N^{\beta,X}_{nmag} + 2\int \Gamma^X(\mathbf{r}_1\alpha, \mathbf{r}_2\beta|\mathbf{r}_1\beta, \mathbf{r}_2\alpha)\, d\mathbf{r}_1\, d\mathbf{r}_2 \tag{3}$$

Θ^X is exact[40] if $\Gamma^X(\mathbf{r}_1\alpha, \mathbf{r}_2\beta|\mathbf{r}_1\beta, \mathbf{r}_2\alpha)$ is the spin-off-diagonal $(\alpha\beta|\beta\alpha)$ element of the exact two-particle density matrix;[38] $N^{\beta,X}_{nmag}$ is the number of paired β electrons, and $N^{\alpha,X} \geq N^{\beta,X}$.

2.2. The EBS + U_{scf} Approach. The problem with the economical GGA functionals is that they suffer severely from self-interaction and thus from an unacceptable overestimation of $|J|$. Keeping an eye on the computational efficiency and acknowledging the excellent performance of the self-consistent linear-response-based GGA+U_{scf} method[29,30] for challenging molecular systems[29,31,33] prompted us to combine this approach with the extended spin-projection scheme. Self-interaction results in an unphysical curvature of the GGA energy curve as a function of "local" electron occupation for noninteger (or fractional) values of local occupation as discussed in detail in ref 30 in the context of Hubbard corrections. Most importantly, by knowing the unphysical curvature of the GGA energy curve, we can repair the self-interaction artifacts of the pure-GGA functional, thus attaining a linear behavior in the GGA energy with respect to the local occupation. The curvature of this function, which is in fact the U parameter, can be obtained conveniently using the linear response approach.[30] The curvature of the GGA energy, or the U parameter, then depends on the system, the definition of "local" occupation, and the density functional that we have chosen. Such a GGA+U functional in turn provides new energy and a new set of orbitals to represent the ground-state density, which can in many cases be qualitatively different from the non-U case. Thus, a self-consistent approach[29] is required to obtain the true numerical U value for the ground-state wave function.

In this spirit, the Hubbard functional[30]

$$E^X_U = \frac{1}{2}\sum_{I,\sigma} U^{I,X}_{scf}\mathrm{Tr}[\mathbf{n}^{I,\sigma}(\mathbf{1} - \mathbf{n}^{I,\sigma})] \tag{4}$$

is added to the GGA functional used within EBS to describe the HS and BS states; I runs over all selected atoms where the Hubbard correction is applied. The occupation matrix $\mathbf{n}^{I,\sigma}$ is

$$n^{I,\sigma}_{j,k} = \sum_i f^\sigma_i \langle\psi^\sigma_i|\chi^I_j\rangle\langle\chi^I_k|\psi^\sigma_i\rangle \tag{5}$$

where the sum runs over all spin orbitals ψ^σ_i with occupation f^σ_i. In the present case, χ^I_j is the set of five orthonormal pseudo atomic d-orbitals of iron atoms.

In addition to providing direct access to J, this two-determinant EBS+U_{scf} approach allows for a convenient and general spin-projected representation of the total energy of the antiferromagnetic LS ground state via

$$E^{LS} = (1 + c)E^{BS} - cE^{HS} = \mathscr{P}E^{BS,HS} \tag{6}$$

$$c = \frac{S_{max} - S_{min} + \Theta^{BS}}{S^2_{max} - S^2_{min} - \Theta^{BS} + \Theta^{HS}} \tag{7}$$

where $\mathscr{P}$ projects the energy of the LS state from the energies of the two single-determinant BS and HS states.[37,38] Having access to the total energy and its derivatives enables spin-projected multideterminant ab initio molecular dynamics via $M_I\ddot{\mathbf{R}}_I = -\nabla_I\mathscr{P}E^{BS,HS}$. We stress that this allows one to compute both $J(t)$ and the geometrical structure of the complexes consistently using the identical spin-projection and electronic structure methods at variance with the standard approach to obtain only J from spin-projection. For convenience, we have used the strong localization approximation of magnetic orbitals for Θ^X as assessed thoroughly in ref 38.

Table 1. Selected Structural Properties (Distances in Å and Angles in deg) of the Fe_2S_2 Core for the Fully Optimized BS, EBS, BS+U_{scf}, and EBS+U_{scf} Structures of the $[Fe_2S_2(SH)_4]^{2-}$ Complex in Vacuo Together with the Exchange Coupling Constant J (Reported in cm $^{-1}$) of These Structures Computed Using Various Methods as Indicated; See "Statics"[a]

	statics				dynamics				
	BS	BS+U	EBS	EBS+U	EBS	EBS+U	EBS @ Fd	EBS+U @ Fd	X-ray @ Fd
r(Fe1−Fe2)	2.68	2.78	2.62	2.72	2.64	2.75	2.62	2.74	2.75
r(Fe1−S1)	2.20	2.24	2.17	2.22	2.18	2.24	2.22	2.27	2.29
r(Fe1−S2)	2.19	2.24	2.17	2.22	2.17	2.24	2.16	2.22	2.23
r(Fe2−S1)	2.20	2.24	2.18	2.22	2.17	2.24	2.22	2.29	2.23
r(Fe2−S2)	2.20	2.25	2.18	2.23	2.18	2.24	2.17	2.24	2.18
θ(Fe1−S1−Fe2)	74.9	76.6	74.2	75.4	74.8	76.0	72.2	74.0	75.1
θ(Fe1−S2−Fe2)	75.1	76.6	74.2	75.3	74.7	76.0	74.3	76.0	76.8
θ(Fe−S−Fe-S)	0.4	0.2	0.1	1.0	0.1	0.0	8.4	9.7	8.7
J_{PBE}	−390	−192	−435	−223	−402 (±50)	−202 (±40)	−386 (±47)	−175 (±35)	−182 (±20)
$J^{[10,10]}_{CAS-CI}$	−43	−30	−51	−36					
$J^{[10,10]}_{MCAS-CI}$	−127	−92	−155	−112					
$J^{[22,16]}_{CASSCF}$	−186	−137	−216	−159					

[a] Thermal averages of the same properties for the same systems as obtained from molecular dynamics simulations are reported for the EBS and EBS+U_{scf} methods again in vacuo and in the protein (denoted EBS @ Fd and EBS+U @ Fd); see "Dynamics". Structural data of Fd and average J values obtained from these simulations are also compared to the X-ray structure[57] (PDB code: 1qt9, see X-ray @ Fd) and to the experimental J value;[54] for the latter, the rmsd in case of simulations and the experimental errors are reported in parentheses, (σ_J).

2.3. Density Functional Calculations. This EBS+U_{scf} method has been implemented in CPMD.[41] The simulations of the $[Fe_2S_2(SH)_4]^{2-}$ complex in vacuo were performed within spin-unrestricted Kohn−Sham DFT using the CPMD code.[41,42] For the EBS and EBS+U calculations, we used the plane wave/pseudopotential formulation[39] of Kohn−Sham DFT together with the PBE functional.[43,44] The core electrons were represented by ultrasoft pseudopotentials[45] with a plane-wave cutoff of 30 Ry. Additional d-projectors were considered for the sulfur atoms, and scalar relativistic corrections and semicore states were taken for Fe. A cubic box of 40 au with finite cluster boundary conditions[46] was used to decouple the negatively charged periodic images.[39]

In the case of the Hubbard corrected EBS+U_{scf} approach, the self-consistent[29] linear-response procedure[30] is used to compute the U_{scf} parameters acting on the two iron atoms separately for the HS and BS states using the optimized EBS equilibrium structure of $[Fe_2S_2(SH)_4]^{2-}$ in vacuo. This yields $U^{HS}_{scf,0} = 3.45$ eV and $U^{BS}_{scf,0} = 3.50$ eV for the two required Kohn−Sham determinants. It is important to note that within this recently introduced framework the Hubbard-U correction is not adjusted such that J fits any experimental data. Rather it is a property that is extracted self-consistently from the underlying electronic structure theory, that is, the PBE density functional together with a plane wave/pseudopotential representation of the orbitals. Furthermore, the "strongly localized" approximation underlies the calculation of J using the EBS and EBS+U_{scf} approaches, which is consistent with the assumptions underlying the Heisenberg Hamiltonian.[47,38]

2.4. Configuration Interaction Calculations. The two wave function-based methods that we used were a conventional CAS-CI (complete active space configuration interaction) and a modified CAS-CI (MCAS-CI) approach. The Bochum suite of open-shell ab initio programs was used for these calculations.[48−51] The first step is a restricted open-shell Hartree−Fock (ROHF) calculation for the HS state of the complex. This yields a set of orthogonal occupied molecular orbitals, with the 10 3d orbitals at the two Fe atoms singly occupied and all other orbitals at the Fe cores, the bridging S^{2-} anions, and the ligands doubly occupied. These orbitals are then used in a subsequent configuration interaction calculation (CAS-CI), in which all possible configurations with 10 electrons in the 10 3d orbitals are included in the active space, that is, CAS-CI(10,10). The basis set used for $[Fe_2S_2(SH)_4]^{2-}$ in vacuo had approximately aVTZ quality (augmented valence triple-ζ with two sets of polarization functions) and consisted of 500 basis functions.

It is well-known[52,53] that J values determined by CAS-CI are by a factor 2−5 too small mainly because the orbitals determined for the covalent (cov) states yield only a poor description for the charge-transfer (ct) configurations. This leads to too large energy denominators in the perturbation estimate:

$$J_{AF} = -\sum_{ct} \frac{\langle \Psi_{cov}|\hat{H}|\Psi_{ct}\rangle^2}{E_{ct} - E_{cov}} \tag{8}$$

for the antiferromagnetic coupling constant J_{AF}, thus yielding too small values of J_{AF}.

Two different schemes have been employed for improving this description. First, we optimized the wave functions for the ct-configurations, which requires nonorthogonal CI. Even this demanding procedure yields only about 70% of J_{AF}. We have therefore used a simple but efficient modification of CAS-CI by introducing a correction R into the energy denominator in eq 8:

$$\Delta\tilde{E} = (E_{ct} - R) - E_{cov} \approx \tilde{U} \tag{9}$$

to account for the relaxation of the ct wave functions, where R is computed by separate CASSCF calculations.[53] This MCAS-CI approach yields J_{AF} in good agreement with elaborate multireference-CI at the cost of economical CAS-CI. Including the bridging S 3p-orbitals in the active space of multireference CASSCF[22, 16] yields J values better than CAS-CI, but they still deviate significantly from MCAS-CI. Thus, the MCAS-CI results in Table 1 are the most reliable wave function-based values for J to date.

Note that we have used the letter "*U*", describing an on-site Coulomb repulsion, in slightly different but closely related contexts. In the Hubbard functional eq 4, U_{scf} prevents the unpaired d-electrons from being too strongly delocalized, thus reducing spurious self-interactions. In MCAS-CI, $\tilde{U}$ is the cov → ct excitation energy. For $[Fe_2S_2(SH)_4]^{2-}$, the unmodified energy denominators are ∼23.0 eV, whereas $R \approx 15.0$ eV, such that the "true" excitation energies amount to $\tilde{U} \approx 8.0$ eV.

2.5. Molecular Dynamics Simulations. The Car−Parrinello molecular dynamics scheme[39,55] was used for performing molecular dynamics simulations in the approximate low-spin (LS) ground state of [2Fe−2S] systems within the EBS, EBS+U_{scf}, and EBS+U_{scf} QM/MM schemes. We employed a recently introduced spin-projected Car−Parrinello Lagrangian for the LS dynamics, which is described in detail in refs 37, 38. Hydrogen masses were substituted by deuterium masses for technical reasons,[39] and a time step of 4 au corresponding to ∼0.12 fs together with a fictitious orbital mass parameter of 500 au was used. The HS and BS Kohn−Sham wave functions were thermostatted separately using Nosé−Hoover chain thermostats[39,56] to keep the orbitals close to their instantaneous ground state. Similarly, the nuclei and atoms in the QM and MM systems, respectively, were connected to separate Nosé−Hoover chain thermostats at 300 K. After equilibration of ∼2−5 ps, trajectories of ∼18 and 8 ps were collected for the in vacuo complex (using both the EBS and the EBS+U_{scf} approaches) and in protein (using EBS+U_{scf} QM/MM), respectively.

2.6. Protein Model and System Setup. The protein model is based on the oxidized *Anabaena* PCC7119 Fd[57] (PDB code: 1qt9, chain B) where standard protonation states of all amino acids were assumed.[37] In addition to the water molecules resolved in the crystal structure, the system was solvated using 13 265 TIP3P water molecules. In addition, 23 Na^+ and 5 Cl^- ions were added to establish charge neutrality of the whole system. The protein was described using the AMBER94 force field,[58] and the partial charges for the [2Fe−2S] core are based on Bader analysis[59] of the electron density of the $[Fe_2S_2(SH)_4]^{2-}$ cluster in vacuo. The nonbonding interactions for Fe were obtained from ref 60, and cysteinyl parameters were used for S.

For our hybrid QM/MM simulations,[37,61,62] we use the efficient CPMD/Gromos interface[63] within the CPMD program package[41,42] both extended by the EBS and EBS+U_{scf} techniques. In addition to including the spin-projection to describe the LS ground state of the antiferromagnetically coupled [2Fe−2S] core, this approach allows for the consistent computation of spin-projected $J(t)$ values "on the fly" along the trajectories at no extra cost.[38] The QM subsystem contained the [2Fe−2S] cluster as well as the S_γ, C_β, and H_β atoms of the four cysteinyl ligands. The dangling bonds at C_β were saturated using capping H atoms constrained to the $C_\alpha-C_\beta$ connecting line. Thus, the QM part of the protein is $[Fe_2S_2(S-CH_3)_4]^{2-}$] carrying a total charge of −2.

As a part of the cysteins connected to the [2Fe−2S] core are treated by QM and the other part by MM, the charges of the MM atoms need to be reparameterized to obtain a total charge of zero separately for the MM part of the cysteines. This is achieved by distributing the residual charge (of +0.09870) on the C_α and H_α atoms because they are mostly screened by the rest of the residues and are not involved in direct interactions with other residues; the charges of C_α and H_α atoms are increased from −0.0351 to 0.0000 and from 0.0508 to 0.1144, respectively.

For incorporating the QM-MM electrostatic interaction, we have chosen the well-established methods provided in ref 63; see also ref 39. In particular, all of the MM atoms lying within 17 Å of the QM region, which includes all of the protein MM atoms and several solvating water molecules, interact directly with the full QM electronic density using screened electrostatics[63] to counteract electron spill-out.[39] In the far field, the partial charges of all of those MM atoms lying beyond 17 Å with respect to the QM region interact with the multipole moments generated from the electronic charge density distribution of the QM system.[63]

3. Results and Discussion

First, the performance of EBS+U_{scf} to compute J is compared to various other approaches in Table 1 for the $[Fe_2S_2(SH)_4]^{2-}$ complex in vacuo. One first notes that the Hubbard-U_{scf} correction leads to an elongation of the Fe−Fe and Fe−S distances by 0.10 and 0.05 Å, respectively, while the Fe−S−Fe angles remain unaffected, ∼(75.0 ± 1)°. A small amount of out of plane bending (about 1°) is observed in the EBS+U_{scf} case, while the rest of the optimized $[Fe_2S_2(SH)_4]^{2-}$ structures feature a nearly planar core. However, a very symmetric planar average structure is obtained from the MD simulations using the EBS+U_{scf} method. As a side remark, we mention that the minimum energy Fe−Fe distance of 2.62 Å determined by Li and Noodleman[64] for the $[Fe_2S_2(SCH_3)_4]^{2-}$] complex using the spin-projected ground-state energy is exactly matching our EBS result obtained from direct energy minimization of the EBS density functional. This is not a surprising result because the EBS functional is based on the same spin projection as employed for the calculations in ref 64.

This structural expansion is connected with a reduction of $|J|$ by only ∼50 cm^{-1} as judged from MCAS-CI; see Table 1. The main effect of the Hubbard correction, however, is an electronic-structure-based reduction of $|J|$ by almost a factor of 2! In particular, the EBS+U_{scf} result for J yields better agreement with the MCAS-CI than the EBS. Here, it is important to stress that using the less compact BS optimized structure, as mostly done in standard J calculations, is intrinsically inconsistent with the spin-projection used to obtain J itself!

As a next step, temperature and thus fluctuation effects on J are assessed via ab initio molecular dynamics at 300 K by computing the probability distribution function, $P(J)$, from $J(t)$ using the EBS and EBS+U_{scf} methods. First, a significant improvement is achieved with EBS+U_{scf}: the average $\langle J \rangle$ is appropriately shifted from about −400 to −200 cm^{-1} when adding the Hubbard correction to the spin-projected PBE functional (see Figure 1). Second, it is crucial to note that the fluctuations σ_J are dramatic: during its dynamics, $J(t)$

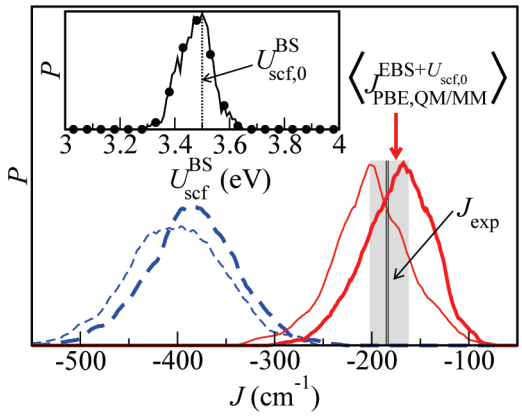

Figure 1. Distribution functions $P(J)$ of $[Fe_2S_2(SH)_4]^{2-}$ in vacuo (thin lines) and of [2Fe−2S] cofactor in *Anabaena* Fd (thick lines) using EBS (dashed blue lines) and EBS+U_{scf} (solid red lines) at 300 K. The value J_{exp} measured in various Fd proteins[66,67,54] is marked by vertical lines and experimental errors[54] by a shaded region, to be compared to the computed average J value in the protein ($J_{PBE,QM/MM}^{EBS+U_{scf,0}}$), marked by the red arrow. The inset shows the distribution function of the linear-response Hubbard-U parameter computed for 100 configurations sampled from 5 ps trajectory of the in vacuo EBS+U_{scf} simulation; $U_{scf,0}^{BS}$ at the EBS equilibrium structure is marked by a vertical line.

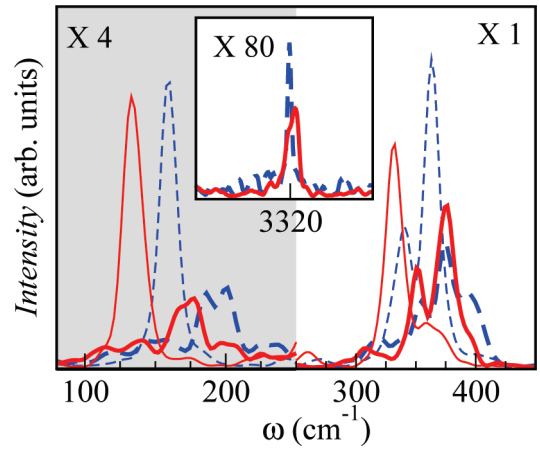

Figure 2. Spectral densities $J(\omega)$ at 300 K of $[Fe_2S_2(SH)_4]^{2-}$ in vacuo (thin lines) and of [2Fe−2S] cofactor in *Anabaena* Fd (thick lines); see Figure 1 for labeling.

spans the range from about −300 to −100 cm^{-1}, thus yielding rmsd values as large as ±40 cm^{-1}; see Table 1.

As a technical note, we extract from the inset of Figure 1 that the value of U_{scf}^{BS} is not strongly dependent on fluctuations at 300 K that drive the complex away from its equilibrium structure and thus from $U_{scf,0}^{BS}$; a similar picture holds for $U_{scf,0}^{HS}$ (not shown). This supports the established procedure[31,33] to compute $U_{scf,0}$ for some reference structure and to keep it fixed during structural relaxation or ab initio molecular dynamics.

In the crucial step of full EBS+U_{scf} QM/MM simulations of the *Anabaena* Fd, |J| is again significantly shifted toward smaller values; see Figure 1. Together with the finite-temperature shift from −223 to −202 cm^{-1} in vacuo and the vacuum-to-protein shift of another ∼30 cm^{-1} at 300 K, the resulting $\langle J \rangle$ value of −175 ± 35 cm^{-1} compares favorably to the experimental values of −183,[66] −185,[67] and −182 ± 20 cm^{-1} [54] measured in vitro for several Fd species that are closely related to the one considered here fully in silico. Thus, a sound electronic structure treatment in conjunction with the protein environment fluctuating at finite temperatures is necessary for a reliable nonempirical computation of average J values in proteins.

Similar to what has been observed for calculations in vacuo, an expansion in the structure of the core has been observed (Table 1). It is interesting to note that structural parameters predicted by the EBS+U_{scf} QM/MM method are closer to the crystal structure[57] than those obtained from the simpler EBS QM/MM scheme. Like in the EBS QM/MM calculations,[37] an asymmetry in the hydrogen-bonding pattern near the iron−sulfur core is also observed in the case of the EBS+U_{scf} QM/MM calculations. The Fe1−S1 (Fe1−S2) and Fe2−S1 (Fe2−S2) bond lengths are nearly the same, while Fe1−S1 (Fe2−S1) and Fe1−S2 (Fe1−S1) are quite different, which is ascribed to the hydrogen bonds to the [2Fe−2S] core within the solvated Fd. Different Fe2−S1 and Fe2−S2 bond lengths between EBS+U_{scf} and the crystal structure can be traced back to a distinct hydrogen-bonding topology near the [2Fe−2S] cofactor as compared to the crystal structure as already amply discussed earlier.[37] This different topology might originate from a combination of solvation and finite temperature effects, which can easily change hydrogen-bonding patterns in view of the small energies involved. In fact, the structural data obtained for synthetic analogues of Fd[65] not only deviate from our calculations, but they also differ from the crystal structure of oxidized *Anabaena* Fd.[57] This is not surprising as the structure of the [2Fe−2S] core varies with its local environment, noting that the synthetic analogues have very different ligands as compared to wild-type Fd; no hydrogen bonds exist with the core, and counterions are present in the cyrstal structure.

Last but not least, having direct access to the dynamics of the exchange coupling, $J(t)$, allows one to evaluate its power spectrum $J(\omega)$ via Fourier transforming its autocorrelation function; see Figure 2. One striking feature, both in vacuo and in protein, is the red-shift or softening of $J(\omega)$ due to the Hubbard correction. A detailed normal-mode analysis[37,38] shows that the two major peaks around 130 and 320 cm^{-1} in vacuo can be solely assigned to $A_{g,A}$ and $A_{g,D}$ vibrational modes involving mainly angles and distances, respectively, of the Fe_2S_2 core. Furthermore, a weak peak at ∼260 cm^{-1} and the shoulder at 350−370 cm^{-1} is due to vibrational coupling with the four SH-ligands. In the protein, however, $J(\omega)$ is systematically blue-shifted with respect to in vacuo as a result of structural constraints on the entire [2Fe−2S] cofactor imposed by the protein. In addition to this trend, the power spectrum $J(\omega)$ is much richer in the protein, which can be traced back to the mutual coupling of [2Fe−2S] motion to various skeleton vibrations. Most strikingly, very high-frequency modulations of $J(\omega)$ at about 3320 cm^{-1} can be related to hydrogen bonding to the core.

4. Conclusion

We introduced a multideterminant QM/MM dynamics approach that combines systematically spin-projection with a

linear-response Hubbard-U_{scf} correction to compute exchange couplings including their time-evolution, $J(t)$, for antiferromagnetic transition metal dimers in complex molecular environments. Studying the [2Fe−2S] cofactor in Ferredoxin as a first example, it is shown that J depends crucially on the subtle interplay of the quality of spin-projection, reduction of self-interaction artifacts, thermal fluctuations, protein matrix shifts, and a consistent treatment of geometrical structure and magnetic coupling. Taking into account all of these effects, consistently EBS+U_{scf} QM/MM simulations are shown to yield excellent agreement with experiment. Transcending the specific case and implementation, the established framework can be generalized to other systems containing antiferromagnetically coupled centers, including polynuclear transition metal complexes, organic radicals, and molecular magnets. Most interestingly, this method can also be applied to magnetic states other than the ground state, which so far are not accessible to molecular dynamics techniques.

Acknowledgment. J.R.-A. is grateful to AvH and Catalan Government for Humboldt and Beatriu de Pinós Fellowships. D.M. acknowledges financial support from DFG (MA 1547/7) and FCI. Calculations were done at NIC (Jülich), Bovilab@RUB (Bochum), and Rechnerverbund-NRW.

References

(1) Willett, R. D.; Gatteschi, D.; Kahn, O. Magneto-Structural Correlations in Exchange Coupled Systems; Reidel: Dordrecht, 1985; pp 1−632.

(2) Pickett, W. E. *Rev. Mod. Phys.* **1989**, *61*, 433–512.

(3) Ribas Gispert, J. *Coordination Chemistry*; Wiley-VCH: Weinheim, 2008; pp 295−338.

(4) Beinert, H.; Holm, R. H.; Münck, E. *Science* **1997**, *277*, 653–659.

(5) Gatteschi, D.; Caneschi, A.; Pardi, L.; Sessoli, R. *Science* **1994**, *265*, 1054–1058.

(6) Wernsdorfer, W.; Sessoli, R. *Science* **1999**, *284*, 133–135.

(7) Mandal, S.; Green, M. A.; Pati, S. K.; Natarajan, S. *J. Mater. Chem.* **2007**, *17*, 980–985.

(8) Schnelzer, L.; Waldmann, O.; Horvatic, M.; Ochsenbein, S. T.; Kraemer, S.; Berthier, C.; Guedel, H. U.; Pilawa, B. *Phys. Rev. Lett.* **2007**, *99*, 087201.

(9) Rees, D. C.; Howard, J. B. *Science* **2003**, *300*, 929–931.

(10) Howard, J. B.; Rees, D. C. *Proc. Natl. Acad. Sci. U.S.A.* **2006**, *103*, 17088–17093.

(11) Pati, S. K.; Mallajosyula, S. S. *Angew. Chem., Int. Ed.* **2009**, *48*, 4977–4981.

(12) Pati, S. K.; Ramasesha, S.; Sen, D. Exact and Approximate Theoretical Techniques for Quantum Magnetism in Low Dimensions. In *Magnetism: Molecules to Materials IV*; Miller, J. S., Drillon, M., Eds.; Wiley-VCH Verlag GmbH & Co.: KGaA Weinheim, Germany, 2002; pp 119−171.

(13) Perdew, J. P.; Zunger, A. *Phys. Rev. B* **1981**, *23*, 5048–5079.

(14) Martin, R. L.; Illas, F. *Phys. Rev. Lett.* **1997**, *79*, 1539–1542.

(15) Svane, A.; Gunnarsson, O. *Phys. Rev. Lett.* **1990**, *65*, 1148–1151.

(16) Filippetti, A.; Fiorentini, V. *Phys. Rev. Lett.* **2005**, *95*, 086405.

(17) Akande, A.; Sanvito, S. *J. Chem. Phys.* **2007**, *127*, 034112.

(18) Rivero, P.; de P. R. Moreira, I.; Illas, F.; Scuseria, G. E. *J. Chem. Phys.* **2008**, *129*, 184110.

(19) Kudin, K. N.; Scuseria, G. E.; Martin, R. L. *Phys. Rev. Lett.* **2002**, *89*, 266402.

(20) Herrmann, C.; Yu, L.; Reiher, M. *J. Comput. Chem.* **2006**, *27*, 1223–1239.

(21) Dederichs, P. H.; Blügel, S.; Zeller, R.; Akai, H. *Phys. Rev. Lett.* **1984**, *53*, 2512–2515.

(22) Wu, Q.; Van Voorhis, T. *Phys. Rev. A* **2005**, *72*, 024502.

(23) Behler, J.; Delley, B.; Lorenz, S.; Reuter, K.; Scheffler, M. *Phys. Rev. Lett.* **2005**, *94*, 036104.

(24) Rudra, I.; Wu, Q.; Van Voorhis, T. *J. Chem. Phys.* **2006**, *124*, 024103−1−9.

(25) Sit, P. H.-L.; Cococcioni, M.; Marzari, N. *Phys. Rev. Lett.* **2006**, *97*, 028303.

(26) Schmidt, J. R.; Shenvi, N.; Tully, J. C. *J. Chem. Phys.* **2008**, *129*, 114110.

(27) Anisimov, V. I.; Zaanen, J.; Andersen, O. K. *Phys. Rev. B* **1991**, *44*, 943–954.

(28) Liechtenstein, A. I.; Anisimov, V. I.; Zaanen, J. *Phys. Rev. B* **1995**, *52*, R5467–R5470.

(29) Kulik, H. J.; Cococcioni, M.; Scherlis, D. A.; Marzari, N. *Phys. Rev. Lett.* **2006**, *97*, 103001.

(30) Cococcioni, M.; de Gironcoli, S. *Phys. Rev. B* **2005**, *71*, 035105.

(31) Sit, P. H.-L.; Cococcioni, M.; Marzari, N. *J. Electroanal. Chem.* **2007**, *607*, 107–112.

(32) Scherlis, D. A.; Cococcioni, M.; Sit, P. H.-L.; Marzari, N. *J. Phys. Chem. B* **2007**, *111*, 7384–7391.

(33) Kulik, H. J.; Marzari, N. *J. Chem. Phys.* **2008**, *129*, 134314.

(34) Noodleman, L. *J. Chem. Phys.* **1981**, *74*, 5737–5743.

(35) Noodleman, L.; Peng, C. Y.; Case, D. A.; Mouesca, J.-M. *Coord. Chem. Rev.* **1995**, *144*, 199–244.

(36) Noodleman, L.; Lovell, T.; Liu, T.; Himo, F.; Torres, R. A. *Curr. Opin. Chem. Biol.* **2002**, *6*, 259–273.

(37) Schreiner, E.; Nair, N. N.; Pollet, R.; Staemmler, V.; Marx, D. *Proc. Natl. Acad. Sci. U.S.A.* **2007**, *104*, 20725–20730.

(38) Nair, N. N.; Schreiner, E.; Pollet, R.; Staemmler, V.; Marx, D. *J. Chem. Theory Comput.* **2008**, *4*, 1174–1188.

(39) Marx, D.; Hutter, J. *Ab Initio Molecular Dynamics: Basic Theory and Advanced Methods*; Cambridge University Press: Cambridge, UK, 2009; pp 1−285.

(40) Wang, J.; Becke, A. D.; Smith, V. H., Jr. *J. Chem. Phys.* **1995**, *102*, 3477–3480.

(41) CPMD, Version 3.11; Copyright IBM Corp. 1990−2009, MPI für Festkörperforschung Stuttgart, 1997−2001.

(42) Marx, D.; Hutter, J. Ab Initio Molecular Dynamics: Theory and Implementation. In *Modern Methods and Algorithms of Quantum Chemistry*; Grotendorst, J., Ed.; John von Neumann Institute for Computing (NIC), Forschungszentrum Jülich: Germany, 2000; Vol. 3, pp 301−449.

(43) Perdew, J. P.; Burke, K.; Ernzerhof, M. *Phys. Rev. Lett.* **1996**, *77*, 3865–3868.

(44) Perdew, J. P.; Burke, K.; Ernzerhof, M. *Phys. Rev. Lett.* **1997**, *78*, 1396–1399.

(45) Vanderbilt, D. *Phys. Rev. B* **1990**, *41*, 7892–7895.

(46) Martyna, G. J.; Tuckerman, M. E. *J. Chem. Phys.* **1999**, *110*, 2810–2821.

(47) Adamo, C.; Barone, V.; Bencini, A.; Broer, R.; Filatov, M.; Harrison, N. M.; Illas, F.; Malrieu, J. P.; de P. R. Moreira, I. *J. Chem. Phys.* **2006**, *124*, 107101.

(48) Staemmler, V. *Theor. Chim. Acta* **1977**, *45*, 89–94.

(49) Wasilewski, J. *Int. J. Quantum Chem.* **1989**, *36*, 503–524.

(50) Meier, U.; Staemmler, V. *Theor. Chim. Acta* **1989**, *76*, 95–111.

(51) Fink, R.; Staemmler, V. *Theor. Chim. Acta* **1993**, *87*, 129–145.

(52) Illas, F.; Casanovas, J.; García-Bach, M. A.; Caballol, R.; Castell, O. *Phys. Rev. Lett.* **1993**, *71*, 3549–3552.

(53) Fink, K. *Chem. Phys.* **2006**, *326*, 297–307.

(54) Petersson, L.; Cammack, R.; Rao, K. K. *Biochim. Biophys. Acta* **1980**, *622*, 18–24.

(55) Car, R.; Parrinello, M. *Phys. Rev. Lett.* **1985**, *55*, 2471–2474.

(56) Martyna, G. J.; Klein, M. L.; Tuckerman, M. *J. Chem. Phys.* **1992**, *97*, 2635–2643.

(57) Morales, R.; Chron, M. H.; Hudry-Clergeon, G.; Petíllot, Y.; Norager, S.; Medina, M.; Frey, M. *Biochemistry* **1999**, *38*, 15764–15773.

(58) Cornell, W. D.; Cieplak, P.; Bayly, C. I.; Gould, I. R.; Merz, K. M.; Ferguson, D. M.; Spellmeyer, D. C.; Fox, T.; Caldwell, J. W.; Kollman, P. A. *J. Am. Chem. Soc.* **1995**, *117*, 5179–5197.

(59) Henkelman, G.; Arnaldsson, A.; Jónsson, H. *Comput. Mater. Sci.* **2006**, *36*, 354–360.

(60) Giammona, D. A. An Examination of Conformational Flexibility in Porphyrins and Bulky-Ligand Binding in Myoglobin. Ph.D. Thesis, University of California, Davis, CA, 1994.

(61) Rousseau, R.; Kleinschmidt, V.; Schmitt, U. W.; Marx, D. *Angew. Chem., Int. Ed.* **2004**, *43*, 4804–4807.

(62) Mathias, G.; Marx, D. *Proc. Natl. Acad. Sci. U.S.A.* **2007**, *104*, 6980–6985.

(63) Laio, A.; VandeVonde, J.; Rothlisberger, U. *J. Chem. Phys.* **2002**, *116*, 6941–6947.

(64) Li, J.; Noodleman, L. Electronic Structure Calculations: Density Functional Methods for Spin Polarization, Charge Transfer, and Solvent Effects in Transition Metal Complexes. In *Spectroscopic Methods in Bioinorganic Chemistry, ACS Symposium Series*; Solomon, E. I., Hodgson, K. O., Eds.; American Chemical Society: Washington, DC, 1998; Vol. 692, pp 179−196.

(65) Mayerle, J. J.; Denmark, S. E.; DePamphilis, B. V.; Ibers, J. A.; Holm, R. H. *J. Am. Chem. Soc.* **1975**, *97*, 1032–1045.

(66) Palmer, G.; Dunham, W. R.; Fee, J. A.; Sands, R. H.; Iizuka, T.; Yonetani, T. *Biochim. Biophys. Acta* **1971**, *245*, 201–207.

(67) Anderson, R. E.; Dunham, W. R.; Sands, R. H.; Bearden, A. J.; Crespi, H. L. *Biochim. Biophys. Acta* **1975**, *408*, 306–318.

CT900547W